Borate-Based Ultraviolet and Deep-Ultraviolet Nonlinear Optical Crystals

Yi Yang [1,2], Xingxing Jiang [1,*], Zheshuai Lin [1,2,*] and Yicheng Wu [1]

1   Center for Crystal R&D, Key Lab of Functional Crystals and Laser Technology of Chinese Academy of Sciences, Technical Institute of Physics and Chemistry, Chinese Academy of Sciences, Beijing 100190, China; yangyi_0424@163.com (Y.Y.); ycwu@mail.ipc.ac.cn (Y.W.)
2   University of the Chinese Academy of Sciences, Beijing 100049, China
*   Correspondence: xxjiang@mail.ipc.ac.cn (X.J.); zslin@mail.ipc.ac.cn (Z.L.); Tel.: +86-10-8254-3718 (Z.L.)

Abstract: Borates have long been recognized as a very important family of nonlinear optical (NLO) crystals, and have been widely used in the laser frequency-converting technology in ultraviolet (UV) and deep-ultraviolet (DUV) regions. In this work, the borate-based UV and DUV NLO crystals discovered in the recent decade are reviewed, and the structure–property relationship in the representative borate-based UV and DUV NLO crystals is analyzed. It is concluded that the optical properties of these crystals can be well explained directly from the types and spatial arrangements of B-O groups. The deduced mechanism understanding has significant implications for the exploration and design of new borate-based crystals with excellent UV and DUV NLO performance.

1. Introduction

In 1961, Franken and his co-workers observed the phenomenon of second-harmonic generation (SHG) in quartz [1]. Since then, nonlinear optics have attracted much attention and developed into one of the key branches of modern optics. A physicochemical phenomenon often leeches onto a material as the carrier, and in turn the materials usually find a practical application, benefiting from the attached property. Without exception, nonlinear optical (NLO) crystals, one of the most important optoelectronic functional material types, are now widely used in laser wavelength-converting technology [2–7]. In particular, the NLO crystals are vital to the generation of coherent light in the ultraviolet (UV, λ < 400 nm) and deep-ultraviolet region (DUV, λ < 200 nm) regions by all-solid-state lasers, owing to its great application in many scientific and engineering fields such as semiconductor photolithography, micromachining and ultraprecise photoelectron spectrometry [8–11]. Therefore, the exploration of NLO crystals in UV and DUV regions has been one of the research hotspots in the field of optoelectronic functional materials for decades.

From the viewpoint of practical applications, for a good UV (and DUV) NLO crystal, the following four conditions must be taken into consideration [12]. Firstly, a short absorption cutoff (λ_{cutoff}) or wide energy bandgap (E_g) is necessary to guarantee the transmittance in the UV and DUV spectra. Moreover, the large bandgap can significantly decrease the occurrence possibility of two-photon absorption or multi-photon absorption by strong laser radiation, and thus great increase the laser-induced damage threshold in crystal. Secondly, the NLO response should be as large as possible for high NLO conversion efficiency. The SHG coefficient (d_{ij}) should be larger than $1 \times$ KDP (KH_2PO_4, $d_{36} \sim 0.39 \times$ pm/V) in the UV and DUV regions. Thirdly moderate birefringence ($\Delta n \sim 0.06$–0.10 @ 400 nm) is important for the achievement of the phase-matching condition if quasi-phase matching is

not available in the crystals [13]. Meanwhile, the refractive indices dispersion in the UV (and DUV) region should be low so as to match the fundamental wave with the SHG light [14]. Finally, good single crystal growth habit, chemical stability and mechanical properties are required.

In borates, the large difference between the electronegativity of boron and oxygen atoms is very favorable for the transmittance of short-wavelength light. Moreover, boron atoms can be three- or four-coordinated with oxygen atoms, forming $(BO_3)^{3-}$ planar triangles and $(BO_4)^{5-}$ polyhedra. The presence of conjugated π-orbital and highly anisotropic electron distribution in the $(BO_3)^{3-}$ group is very beneficial to the generation of large microscopic second-order susceptibility and birefringence [15]. The elimination of dangling bonds on the oxygen anions in the B-O groups can effectively increase the energy bandgap and make the absorption edge blue-shifted in the borate crystals [14,15]. The spatial combinations of $(BO_3)^{3-}$ and $(BO_4)^{4-}$ groups contribute the diverse structural types in borate-based compounds. In the 1980s, two important NLO borates, β-BaB_2O_4 (BBO) [16,17] and LiB_3O_5 (LBO) [18], were discovered. These two crystals exhibit the excellent NLO performance in the visible and UV regions. Nevertheless, the relatively narrow energy bandgap (E_g ~ 6.5 eV or λ_{cutoff} ~190 nm) in BBO and the small birefringence value (Δn ~0.04 @ 400 nm) in LBO restrict their applications in the DUV region. In the 1990s, another important NLO borate $KBe_2BO_3F_2$ (KBBF) [19–22] was discovered in Chen's group. This crystal, and its analogs $RbBe_2BO_3F_2$ (RBBF) [23] and $CsBe_2BO_3F_2$ (CBBF) [24], possess a very large energy bandgap (E_g ~8.3 eV) and a relatively strong SHG effect (~1.2 × KDP). Moreover, the birefringence values for the three crystals are about 0.07 ~ 0.08 @ 400 nm, and the shortest SHG phase-matching wavelengths are 161 nm, 170 nm and 201 nm for KBBF, RBBF and CBBF, respectively [25]. This clearly indicates the excellence for the KBBF family crystals used as the DUV NLO crystals. However, due to the weak interaction between alkali metal and fluorine cations, the layering growth habit in the KBBF family crystals brings significant difficulty to single crystal growth and severely hiders their practical applications. Therefore, the explorations for new borate-based crystals with good UV (especially DUV) NLO performances are greatly desirable.

Since the beginning of this century, quite a few new borate-based UV or DUV NLO compounds have been synthesized. They exhibit wide energy bandgaps and large NLO effects accompany with the diverse structural features. Considering that the number of UV and DUV NLO borates is still in a very small ratio compared with the whole number of borate compounds, it is important to know how microscopic structures determine the optical properties in these optoelectronic functional materials. In this review, we will focus on the developments of the borate-based UV and DUV NLO crystals in the recent decade. Some representative borate compounds are chosen according to the variability of microscopic B-O groups, and their structure–property relationship is analyzed. Based on the analysis and summarization, the prospects for UV and DUV NLO borates are discussed.

2. Results and Discussion

The space group, UV edge, SHG effect and birefringence of all the mentioned representative borate-based UV and DUV NLO crystals are listed in Table 1.

2.1. Borate Crystals in Which the B-O Groups Are $(BO_3)^{3-}$ Groups Only

According to their structural features, the types of borates discovered in the recent decade can mainly be catalogued into three classes: KBBF-type, $Sr_2Be_2B_2O_7$ (SBBO)-type and three-dimensional network crystals. In most of these crystals, the NLO properties are mainly attributed to the $(BO_3)^{3-}$ groups.

2.1.1. KBBF-Type Crystals

$KBe_2BO_3F_2$ (KBBF) is the unique NLO crystal that can generate coherent light at wavelengths below 200 nm by direct SHG method [22,26–29]. KBBF possesses a layer structure (Figure 1). Each terminal oxygen atom of the $(BO_3)^{3-}$ groups is shared with two $(BeO_3F)^{5-}$ tetrahedra, forming

an infinite $[Be_2BO_3F_2]_\infty$ layer. The layers are connected by electrostatic interaction between potassium and fluorine ions. Herein, the KBBF-type crystals are referred to the crystals in which the terminal oxygen atoms of $(BO_3)^{3-}$ groups are exclusively connected with two (MO_3X) (M = Be and Zn, X = F, Cl and Br) tetrahedra in the ratio 1:2 to form the $[M_2BO_3X_2]_\infty$ layer, and the layers are linked by weak ionic bonds.
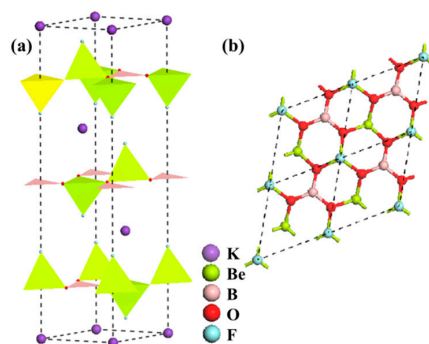
Figure 1. (**a**) The crystal structure of the $KBe_2BO_3F_2$ (KBBF) crystal and (**b**) $[Be_2BO_3F_2]_\infty$ layer. $(BO_3)^{3-}$ and $(BeO_3F)^{5-}$ groups are represented by pink and green polyhedra respectively.

$BaBe_2BO_3F_3$ (BBBF):

Much effort has been devoted to overcome the layering habit of KBBF family crystals. In 2016, Guo et al. proposed the strategy to improve the growth habit by enhancing electrostatic interaction, and successfully synthesized $BaBe_2BO_3F_3$ (BBBF) [30]. BBBF crystallizes in hexagonal space group of $P6_3$. In one unit cell, two $[Be_2BO_3F_2]_\infty$ layers in KBBF are aligned vertical to c-axis in a nearly antiparallel manner, and the barium cations are located between the interstice between the layers (Figure 2). At the same time, isolated fluorine anions are also introduced to compensate the valence imbalance resulting from the substitution K^+ with Ba^{2+} ions. Based on simple Coulomb model, the electrostatic interaction between the $[Be_2BO_3F_2]_\infty$ layer and interstitial cations of BBBF is 1.5 times that of KBBF, indicating that the layered habit is largely overcome in BBBF. Benefiting from large birefringence originating from the parallel arrangement of $(BO_3)^{3-}$ plane, the phase-matching ability evaluation based on the first-principles refractive indices calculations revealed that the shortest SHG wavelength is 196 nm, implying that BBBF could be truly used in the SHG in the DUV region. However, suffering from the nearly antiparallel alignment of $(BO_3)^{3-}$ groups, the powder SHG response of BBBF is just $0.1 \times$ KDP.
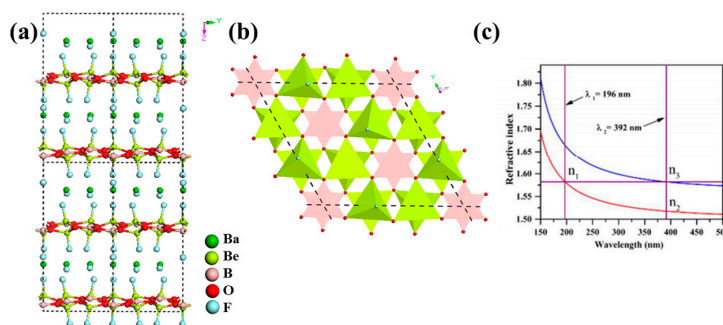
Figure 2. (**a**) The structure of $BaBe_2BO_3F_3$ (BBBF). (**b**) The adjacent $[Be_2BO_3F_2]_\infty$ layers, the $(BO_3)^{3-}$ and $(BeO_3F)^{5-}$ groups are represented by pink and green polyhedra respectively. (**c**) Phase-matching capabilities for BBBF. Adapted and reprinted with permission from ref [30], Copyright 2016 American Chemical Society.

AZn$_2$BO$_3$X$_2$ (A = K, Rb, NH$_4$; X = Cl, Br)

AZn$_2$BO$_3$X$_2$ (A = K, Rb, NH$_4$; X = Cl, Br can be regarded as the production of the "transgenosis" on KBBF crystals) [31,32]. In the "transgenosis" process, potassium cations are replaced by A (K$^+$, Rb$^+$ or NH$_4^+$) ions, and (BeO$_3$F)$^{5-}$ groups are replaced by (ZnO$_3$X)$^{5-}$ tetrahedra (Figure 3). Due to the introduction of (ZnO$_3$X)$^{5-}$ tetrahedra, the shortest absorption edge of AZn$_2$BO$_3$X$_2$ are red-shifted to 190–214 nm. For the same reason, "transgenosis" process doubles the SHG effect of AZn$_2$BO$_3$X$_2$ compared with KBBF, and the mechanism analysis revealed that (ZnO$_3$X)$^{5-}$ tetrahedra dominantly contributes to the SHG effect in the series of materials. This is the first case where [ZnO$_3$Cl/Br] groups can be used as the NLO-active structural units in NLO materials. More importantly, in NH$_4$Zn$_2$BO$_3$X$_2$, the hydrogen bonds between ammonia and halogen ions largely reduce the layered habit and improve the growth habit.
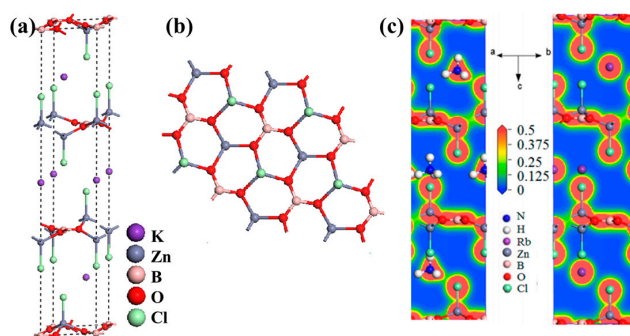
Figure 3. (**a**) Crystal structure of KZn$_2$BO$_3$Cl$_2$, (**b**) the layers of [Zn$_2$BO$_3$Cl$_2$]$_\infty$, (**c**) the electronic densities of NH$_4$Zn$_2$BO$_3$Cl$_2$ and RbZn$_2$BO$_3$Cl$_2$. Adapted and reprinted with permission from ref [32], Copyright 2016 American Chemical Society.

2.1.2. SBBO-Type Crystals

Sr$_2$Be$_2$B$_2$O$_7$ (SBBO) was designed by molecule engineering method in 1995 [33,34]. In the crystal structure of SBBO (Figure 4), the terminal oxygen atoms of (BO$_3$)$^{3-}$ group are bonded with one beryllium atoms, forming a [BeBO$_3$O]$_\infty$ single layer. Two [BeBO$_3$O]$_\infty$ single layers connect each other via the bridge oxygen atoms, forming the [Be$_2$B$_2$O$_7$]$_\infty$ double layers, and the strontium cations are intercalated in the interstices within and between the [Be$_2$B$_2$O$_7$]$_\infty$ double layers. Herein the SBBO-type crystals are referred to the crystals with [M$_2$B$_2$O$_6$X]$_\infty$-type double layers, and the A-site cations are embedded in the interspace inter- or intra-double layers. The measurement based on powder samples revealed that SBBO has the potential for DUV NLO crystals. However, the problem of structure instability has been always an issue for SBBO, which severely hinders its practical application [33,35,36].
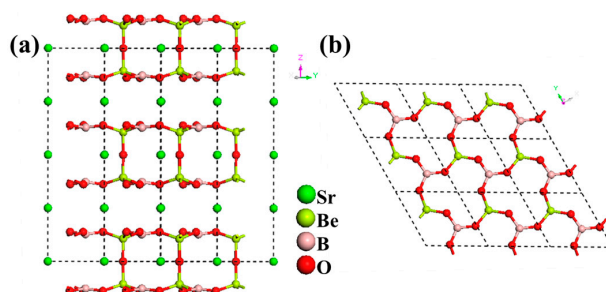

Figure 4. (**a**) The structure of Sr$_2$Be$_2$B$_2$O$_7$ (SBBO) crystal, (**b**) the [Be$_3$B$_3$O$_6$]$_\infty$ layer.

NaCaBe$_2$B$_2$O$_6$F

NaCaBe$_2$B$_2$O$_6$F crystallizes in the monoclinic space group *Cc*, exhibiting an two-dimensional [Be$_2$B$_2$O$_6$F]$_\infty$ double-layer structure, with bridge oxygen in the double layer of SBBO substituted by fluorine atoms [37]. The sodium ions are intercalated in the interstice within [Be$_2$B$_2$O$_6$F]$_\infty$ double layer, while calcium ions are embedded in the cavity between the double layers (Figure 5). Transmittance test revealed that the absorption edge of NaCaBe$_2$B$_2$O$_6$F is 185 nm, resulting from the incomplete elimination of dangling bonds at oxygen atoms. In the lattice, the (BO$_3$)$^{3-}$ groups are aligned in nearly antiparallel orientation, and the geometrical offset of microscopic second-order susceptibility results in a small powder SHG effect about one third that of KDP.
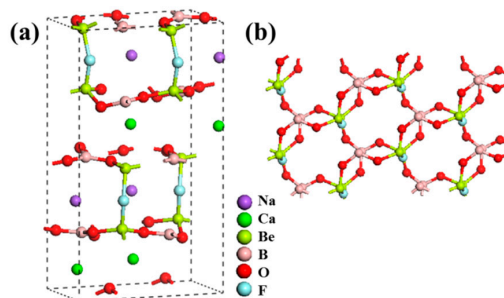
Figure 5. (**a**) The structure of NaCaBe$_2$B$_2$O$_6$F, (**b**) double-layer structure viewed along the *c*-axis.

K$_3$Ba$_3$Li$_2$Al$_4$B$_6$O$_{20}$F

K$_3$Ba$_3$Li$_2$Al$_4$B$_6$O$_{20}$F crystallizes in hexagonal space group *P*-62c. Its exhibits the most complicated [Li$_2$Al$_4$B$_6$O$_{20}$F]$_\infty$ double-layer structure (Figure 6) in the SBBO-type crystals[38]. [Li$_2$Al$_4$B$_6$O$_{20}$F]$_\infty$ double layers are generated by substituting one third of (BeO$_4$)$^{6-}$ with (LiO$_3$F)$^{6-}$ tetrahedra and two thirds of (BeO$_4$)$^{6-}$ with (AlO$_4$)$^{5-}$ tetrahedra. Regardless of the complicated crystal structure, it keeps the similar spatial arrangement of (BO$_3$)$^{3-}$ groups in SBBO, and exhibits a strong SHG effect (1.5 × KDP). Due to the introduction of lithium with low electronegativity and valence in [Li$_2$Al$_4$B$_6$O$_{20}$F]$_\infty$ layers, the nonbonding orbitals of some oxygen atoms are almost reserved, and the absorption edge of K$_3$Ba$_3$Li$_2$Al$_4$B$_6$O$_{20}$F is located at 190 nm. At the same time, the element substitution preserve the strong interaction between [Li$_2$Al$_4$B$_6$O$_{20}$F]$_\infty$ double layers, and K$_3$Ba$_3$Li$_2$Al$_4$B$_6$O$_{20}$F shows no layered habit in the crystal growth process. More importantly, it should be emphasized that the insertion of lithium largely improves the flexibility of [Li$_2$Al$_4$B$_6$O$_{20}$F]$_\infty$ double layers, making it accommodate large K$^+$ ions. Therefore, the problem of structural instability of SBBO is completely eliminated in K$_3$Ba$_3$Li$_2$Al$_4$B$_6$O$_{20}$F, as demonstrated by the phonon spectrum (Figure 6b).
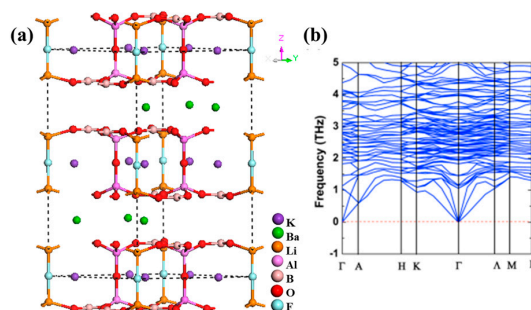
Figure 6. (**a**) Structure of K$_3$Ba$_3$Li$_2$Al$_4$B$_6$O$_{20}$F, (**b**) phonon spectrum of K$_3$Ba$_3$Li$_2$Al$_4$B$_6$O$_{20}$F. Adapted and reprinted with permission from ref [38], Copyright 2016 American Chemical Society.

$Rb_3Al_3B_3O_{10}F$

$Rb_3Al_3B_3O_{10}F$ crystallizes in the trigonal space group of $P3_1c$, and possess a three-dimensional structure (Figure 7, ref [39]). Each $(BO_3)^{3-}$ is linked with one $(AlO_3F)^{4-}$ and two $(AlO_4)^{5-}$ tetrahedra, forming the alveolate $[Al_3(BO_3)_3OF]_\infty$ layer in the (a,b) plane. The apical O/F atoms of (AlO_4/AlO_3F) tetrahedra pointing upward and download are shared by the adjacent layer to serve as the interlayer bridge, constructing the three-dimensional framework. Rubidium cations reside in the interstice of the framework to counterbalance the valence states. UV−vis near-infrared diffuse spectrum revealed that the absorption of $Rb_3Al_3B_3O_{10}F$ is below 200 nm, consistent with the coordination with aluminum of the dangling oxygen atoms in the $(BO_3)^{3-}$ group. Induced by the direct connection of the $[Al_3(BO_3)_3OF]_\infty$ layer, the high spatial density compensates the deterioration of crossing arrangement of $(BO_3)^{3-}$ groups to the SHG response, and the powder SHG effect is about $1.2 \times$ KDP. Moreover, owing to the strong adhesion force of Al-O/F bond between $[Al_3(BO_3)_3OF]_\infty$ layer, no layered habit is observed in the growth of $Rb_3Al_3B_3O_{10}F$.
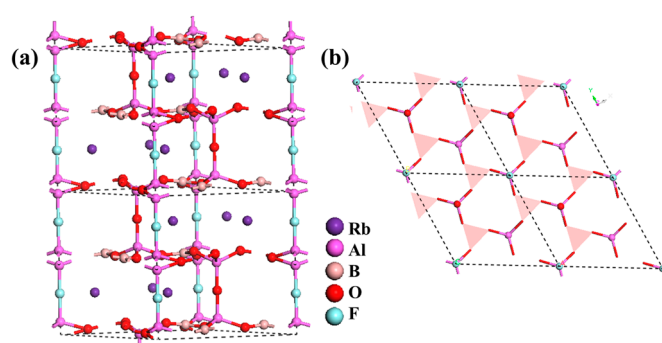

Figure 7. (**a**) Crystal structure of $Rb_3Al_3B_3O_{10}F$, (**b**) the $[Al_3(BO_3)_3OF]_\infty$ layer, the $(BO_3)^{3-}$ groups are represented by pink triangle.

2.1.3. Three-Dimensional (3D) Network Crystals

In this type of borate crystals, the $(BO_3)^{3-}$ groups are connected with other groups to form the 3D networks.

$LiSr(BO_3)_2$

$LiSr(BO_3)_2$ crystallizes in monoclinic space group Cc, which shows a three-dimensional framework structure. Strontium atom is eight-coordinated with oxygen atoms, forming $(SrO_8)^{14-}$ polyhedral [40]. The $(BO_3)^{3-}$ triangles and $(SrO_8)^{14-}$ polyhera are alternatively connected in the ratio of 1:1, constructing the infinite $[SrBO_3]_\infty$ layer. Meanwhile, the strontium atoms are bonded with the oxygen atoms of the $(BO_3)^{3-}$ groups outside of $[SrBO_3]_\infty$ layer and connect the layer together, giving rise to the three-dimensional $[SrB_2O_6]_\infty$ network (Figure 8). The lithium ions are inserted in the interstice within the $[SrB_2O_6]_\infty$ network to keep the electron neutrality. One dangling oxygen atom is left at the $(BO_3)^{3-}$ groups outside of $[SrBO_3]_\infty$ layer, so the absorption edge of $LiSr(BO_3)_2$ just ends at 186 nm. The $(BO_3)^{3-}$ groups within the $[SrBO_3]_\infty$ layer are aligned in a nearly parallel manner, while the outside $(SrBO_3)_\infty$ layers are almost arranged in an antiparallel configuration. Therefore, the "effective" $(BO_3)^{3-}$ groups are those in the $[SrBO_3]_\infty$ layer, and high spatial density of those $(BO_3)^{3-}$ groups results in the large SHG response ($2 \times$ KDP) of $LiSr(BO_3)_2$. Meanwhile, the ordered arrangement of $(BO_3)^{3-}$ groups within the $[SrBO_3]_\infty$ layer also give rise to the large birefringence (0.056, calculated value), making $LiSr(BO_3)_2$ a potential NLO crystal for the output of the 266-nm coherent laser.
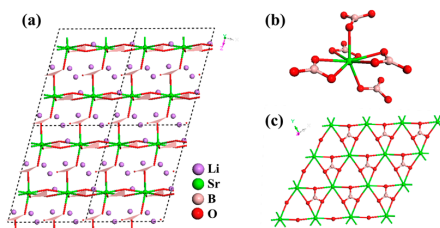
Figure 8. (**a**) The structure of the LiSr(BO$_3$)$_2$ crystal and the (BO$_3$)$^{3-}$ groups are represented by pink triangle, (**b**) (BO$_3$)$^{3-}$ groups coordinated to a (SrO$_8$)$^{14-}$ polyhedron, (**c**) the [SrBO$_3$]$_\infty$ layer.

NaSr$_3$Be$_3$B$_3$O$_9$F$_4$

NaSr$_3$Be$_3$B$_3$O$_9$F$_4$ crystallizes in trigonal space group *R3m*. By sharing the fluorine ions, three (BeO$_3$F)$^{5-}$ tetrahedra constituted a (Be$_3$O$_{12}$F)$^{19-}$ cluster (Figure 9, ref [41]). The oxygen atoms of (Be$_3$O$_{12}$F)$^{19-}$ cluster are connected by three (BO$_3$)$^{3-}$ groups, forming (Be$_3$B$_3$O$_{12}$F)$^{10-}$ building block. In the (Be$_3$B$_3$O$_{12}$F)$^{10-}$ building block, the (BO$_3$)$^{3-}$ are almost parallel with each other, except the slight deviation from (a,b) plane. The (Be$_3$B$_3$O$_{12}$F)$^{10-}$ building blocks are interconnected in almost the same orientation, generating the 3D network. The Na$^+$ and Sr^{2+} are located in the cavity of the 3D network. The absorption edge of NaSr$_3$Be$_3$B$_3$O$_9$F$_4$ is 170nm, originating from single-coordination of oxygen atoms of (BO$_3$)$^{3-}$ groups with beryllium atoms. The subparallel geometry of (BO$_3$)$^{3-}$ groups in the lattice leads to a large SHG response (4~5 × KDP) and birefringence (0.061@400 nm), showing potential for UV NLO crystals for the generation of coherent laser at 266 nm as with LiSr(BO$_3$)$_2$.
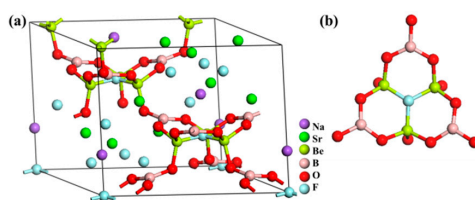
Figure 9. (**a**) The structure of NaSr$_3$Be$_3$B$_3$O$_9$F$_4$, (**b**) the (Be$_3$B$_3$O$_{12}$F)$^{10-}$ cluster.

NaBeB$_3$O$_6$

NaBeB$_3$O$_6$ crystallizes in orthorhombic space group *Pna2$_1$* [42]. By sharing the corner oxygen atoms, three (BO$_3$)$^{3-}$ triangles and two (BeO$_4$)$^{6-}$ tetrahedra form nearly coplanar double six-membered ring (Be$_2$B$_3$O$_{11}$)$^{9-}$ anions, similar to naphthalene. The (Be$_2$B$_3$O$_{11}$)$^{9-}$ building blocks are connected with each other in a crossed manner by sharing the (BeO$_4$)$^{6-}$, forming the endless cruciate chains along the c-axis. The adjacent cruciate chains are connected to each other via sharing the O atoms of (BO$_3$)$^{3-}$ triangles generating the open framework with Na$^+$ ions residing in the tunnels (Figure 10). UV−Vis−NIR diffuse reflectance spectrum revealed that NaBeB$_3$O$_6$ exhibits good transmittance below 200 nm. The (Be$_2$B$_3$O$_{11}$)$^{9-}$ triangles result the very condensed spatial arrangement of (BO$_3$)$^{3-}$ groups, leading to the large SHG response (1.6 × KDP). More importantly, it should be noted that the collinear alignment of NaBeB$_3$O$_6$ also gives rise to the large birefringence (0.08@400 nm, calculated values [14]), which is the first case in borate-based NLO crystals.
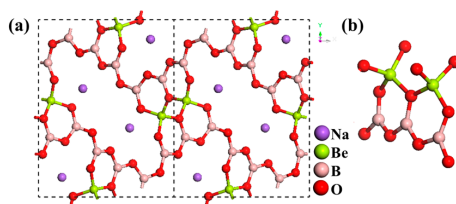

Figure 10. (**a**) The structure of NaBeB$_3$O$_6$, (**b**) double six-membered ring (Be$_2$B$_3$O$_{11}$)$^{9-}$ anions.

Na$_2$Be$_4$B$_4$O$_{11}$ and LiNa$_5$Be$_{12}$B$_{12}$O$_{33}$

One strategy to overcome the layering habit of KBBF is the introduction of the B-O groups interconnecting the 2D [Be$_2$BO$_3$X$_2$] layers. Accordingly, several borate NLO compounds have been discovered, including Na$_2$Be$_4$B$_4$O$_{11}$ [43], LiNa$_5$Be$_{12}$B$_{12}$O$_{33}$ [43], γ-KBe$_2$B$_3$O$_7$ [42], β-KBe$_2$B$_3$O$_7$ [42], RbBe$_2$B$_3$O$_7$ [42] and Na$_2$CsBe$_6$B$_5$O$_{15}$ [44]. Herein, Na$_2$Be$_4$B$_4$O$_{11}$ and LiNa$_5$Be$_{12}$B$_{12}$O$_{33}$ are chosen as the representative examples.

Na$_2$Be$_4$B$_4$O$_{11}$ and LiNa$_5$Be$_{12}$B$_{12}$O$_{33}$ crystallize in triclinic space groups *P*1 and *Pc*, respectively. Regardless of the different macroscopic symmetry, Na$_2$Be$_4$B$_4$O$_{11}$ and LiNa$_5$Be$_{12}$B$_{12}$O$_{33}$ share the similar 3D framework structure. The (BO$_3$)$^{3-}$ group shares each oxygen atom with two (BeO$_4$)$^{6-}$ tetrahedra, forming the infinite two-dimensional [Be$_2$BO$_5$]$_\infty$ layers. The adjacent [Be$_2$BO$_5$]$_\infty$ layers are further bridged together through distorted (B$_2$O$_5$)$^{4-}$ groups by sharing O atoms to build the 3D framework, with the sodium or lithium cations residing in the tunnel of the framework (Figure 11). Despite the absolute elimination of the dangling bonds of the oxygen atoms within the [Be$_2$BO$_5$]$_\infty$ layer, the terminal oxygen atoms of (B$_2$O$_5$)$^{4-}$ are only bonded with one beryllium atoms, leaving some nonbonding orbitals. Therefore, Na$_2$Be$_4$B$_4$O$_{11}$ and LiNa$_5$Be$_{12}$B$_{12}$O$_{33}$ exhibit the absorption edge at 171 and 169 nm respectively. The (BO$_3$)$^{3-}$ groups within (B$_2$O$_5$)$^{4-}$ groups are almost aligned head-to-head in a crossing manner, and they contribute almost nothing to the SHG effect and birefringence. However, on the other hand, the connection of [Be$_2$BO$_5$]$_\infty$ layers via (B$_2$O$_5$)^4 groups largely preserve high density of the effective (BO$_3$)$^{3-}$ group for SHG effect and birefringence. Therefore, both Na$_2$Be$_4$B$_4$O$_{11}$ and LiNa$_5$Be$_{12}$B$_{12}$O$_{33}$ show high SHG efficiency (1.3 and 1.4 times that of KDP, respectively) and phase-matching ability.
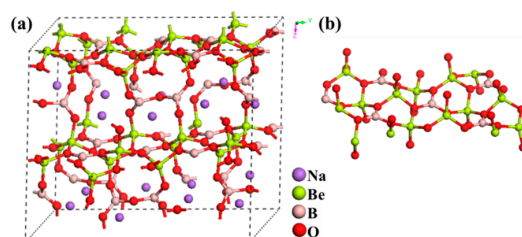
Figure 11. (**a**) the structures of Na$_2$Be$_4$B$_4$O$_{11}$, (**b**) the 2D infinite planar [Be$_2$BO$_5$]$_\infty$ layer.

CsZn$_2$B$_3$O$_7$

CsZn$_2$B$_3$O$_7$ crystallizes in orthorhombic space group *Cmc*2$_1$ [45,46]. Its structure can be regarded as the variant of γ-KBe$_2$B$_3$O$_7$ [42] with beryllium and potassium substituted by zinc and cesium atoms (Figure 12). Due the introduction of zinc atoms with *d*-orbital, the absorption edge of CsZn$_2$B$_3$O$_7$ is red-shifted to 218 nm. Moreover, it also should be noted that (ZnO$_4$)$^{6-}$ also has a considerable contribution to the SHG effect and enhances the SHG effect to 1.5 × KDP (that of γ-KBe$_2$B$_3$O$_7$ is 0.68 KDP).
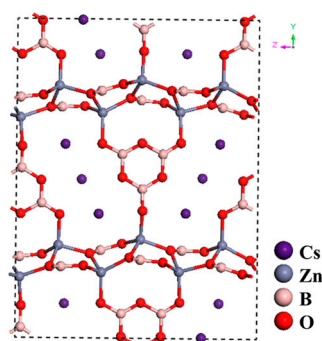

Figure 12. The structure of CsZn$_2$B$_3$O$_7$.

2.2. Borate Crystals in Which the B-O Groups Are (BO$_4$)$^{5-}$ Groups Only

The most famous NLO borates in which the B-O groups are (BO$_4$)$^{5-}$ groups are BPO$_4$ [47–50] and SrB$_4$O$_7$ [51–54]. Both of them have very large energy bandgap (E_g ~9.5 eV) or extremely short absorption edge (λ_{cutoff} ~130 nm). However, due to very small optical anisotropy in (BO$_4$)$^{5-}$ groups, this type of UV NLO borates has too small a birefringence (typically $\Delta n < 0.01$) to achieve the phase-matching condition, and has been less focused on in the recent decade. To our best knowledge, the only known compound in this type of borates is LaBeB$_3$O$_7$, which was synthesized in 2013.

LaBeB$_3$O$_7$

LaBeB$_3$O$_7$ crystallizes in the orthorhombic space group *Pnm*2$_1$ [55]. Two symmetrically independent B sites exist in the lattice. The B(1) sites are fully occupied by boron atoms, while B(2) sites are disordered occupied by boron and beryllium atoms in the molar ratio of 1:1. Via sharing the corner oxygen atoms, two (B(1)O$_4$)$^{5-}$ tetrahedra form an (B$_2$O$_7$)$^{9-}$ dimmer. (XO$_4$) (X = B and Be) tetrahedra are connected by the (B$_2$O$_7$)$^{9-}$ dimmer, and give rise to the three-dimensional network with lanthanum cations located at the channel of the framework (Figure 13). The anionic tetrahedra are aligned almost in the same direction. Regardless of the small second-order susceptibility of (BO$_4$)$^{5-}$ groups, the favorable superposition also results in the relatively large SHG response (1 ~ 2 × KDP). Moreover, the powder SHG test revealed that LaBeB$_3$O$_7$ is phase-matching for the light at 1064 nm. It is speculated that the Be/B disorder occupation brings about a relatively large birefringence (0.03@1634 nm) and improves the phase-matching ability.
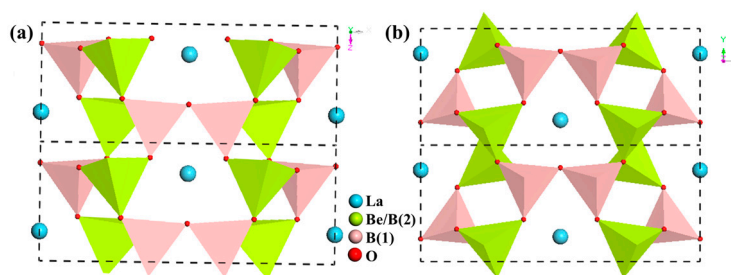
Figure 13. The structure of LaBeB$_3$O$_7$ along (**a**) [010] direction and (**b**) [001] direction. The ((Be/B(2))O$_4$) group is represented by green tetrahedron and the (B(1)O$_4$)$^{5-}$ group is represented by pink tetrahedron.

2.3. Borate Crystals Containing the B-O Combinational Groups

In some UV and DUV NLO borates synthesized in the last decade, the B-O groups are not merely (BO$_3$)$^{3-}$ groups or (BO$_4$)$^{5-}$ groups, but the combination of these two types of basic B-O groups. In this section, several representative NLO compounds in this type of borates are selected. The combinational B-O groups can also result in the good NLO properties of borate crystals in the UV and even DUV regions.

K$_3$B$_6$O$_{10}$Br and K$_3$B$_6$O$_{10}$Cl with (B$_6$O$_{13}$)$^{8-}$

K$_3$B$_6$O$_{10}$Br and K$_3$B$_6$O$_{10}$Cl crystallize in space groups of trigonal *R3m*, and the crystals with different halogen anions are isostructural with each other [56,57]. By sharing the common (BO$_4$)$^{5-}$, their (B$_3$O$_8$)$^{7-}$ groups are interconnected with each other, forming the (B$_6$O$_{13}$)$^{8-}$ building block. (B$_6$O$_{13}$)$^{8-}$ groups are further connected, generating the 3D framework, with potassium and halogen ions located in the interstice of the framework (Figure 14). Except some slant off the (a,b) plane, almost all the (BO$_3$)$^{3-}$ groups are aligned in the same orientation. The favorable superposition of second-order susceptibility and optical anisotropic bring about the large SHG response and birefringence [58–60]. Moreover, the partial elimination of dangling bonds at oxygen atoms result in the good transmittance in DUV region with the absorption 180 nm [60] and 182 nm [58] for K$_3$B$_6$O$_{10}$Cl and K$_3$B$_6$O$_{10}$Br

respectively. All these properties indicate that $K_3B_6O_{10}X$ could be a good candidate for second- and third-harmonic generation for laser at 1064 nm [61,62].

Table 1. The ultraviolet (UV) edge, second-harmonic generation (SHG) coefficients and birefringence value of borate-based nonlinear optical (NLO) compounds.

Chemical Formula (Abbreviation)	Space Group	UV Edge (nm)	SHG Coefficient (pm/V) or Powder SHG Efficiency	Δn(@1064 nn)
Borate crystal in which B-O groups are $(BO_3)^{3-}$ only				
$KBe_2BO_3F_2$ (KBBF) [20]	$R32$	147 [26]	$d_{11} = 0.49$ [68]	0.077 [36]
$CsBe_2BO_3F_2$ (CBBF) [24]	$R32$	151	$d_{11} = 0.50$	0.058
$RbBe_2BO_3F_2$ (RBBF) [23]	$R32$	152	$d_{11} = 0.45 \pm 0.01$	0.073(@694.3 nm)
$BaBe_2BO_3F_3$ (BBBF) [30]	$P6_3$	147(cal)	$0.32 \times KDP$	0.081(cal@200 nm)
$NH_4Zn_2BO_3Cl_2$ [32]	$R32$	190	$2.82 \times KDP$	-
$KZn_2BO_3Cl_2$ [32]	$R32$	194 [32] (~200) [31]	$3.01 \times KDP$ [32] $1.3 \times KDP$ [31]	-
$RbZn_2BO_3Cl_2$ [31,32]	$R32$	198 [32]	$2.85 \times KDP$ [32] $1.17 \times KDP$ [31]	-
$KZn_2BO_3Br_2$ [31,32]	$R32$	209 [32]	$2.68 \times KDP$ [32]	-
$RbZn_2BO_3Br_2$ [31,32]	$R32$	214 [32]	$2.53 \times KDP$ [32]	-
$Sr_2Be_2B_2O_7$ (SBBO) [33]	$P\text{-}6c2$	155	$d_{22} = 2.0\text{-}2.48$	0.062(@589 nm)
$NaCaBe_2B_2O_6F$ [37]	Cc	190	$1/3 \times KDP$	
$K_3Ba_3Li_2Al_4B_6O_{20}F$ [38]	$P\text{-}62c$	190	$1.5 \times KDP$	0.052(cal@532 nm)
$Rb_3Al_3B_3O_{10}F$ [39]	$P3_1c$	< 200	$1.2 \times KDP$	-
$LiSr(BO_3)_2$ [40]	Cc	186	$d_{eff} = 0.76$ $2 \times KDP$	0.056(cal)
$NaSr_3Be_3B_3O_9F_4$ [41]	$R3m$	170	$5 \times KDP$	0.06
$NaBeB_3O_6$ [42]	$Pna2_1$	170(cal) [14]	$d_{eff} = 0.62$ $1.6 \times KDP$	
$Na_2Be_4B_4O_{11}$ [43]	$P1$	171	$1.3 \times KDP$	-
$LiNa_5Be_{12}B_{12}O_{33}$ [43]	Pc	169	$1.4 \times KDP$	-
γ-$KBe_2B_3O_7$ [42]	$P2_1$	186(cal) [14]	$d_{eff} = 0.27$ $0.68 \times KDP$	
β-$KBe_2B_3O_7$ [42]	$Pmn2_1$	187(cal) [14]	$d_{eff} = 0.29$ $0.75 \times KDP$	
$RbBe_2B_3O_7$ [42]	$Pmn2_1$	179(cal) [14]	$d_{eff} = 0.31$ $0.79 \times KDP$	
$Na_2CsBe_6B_5O_{15}$ [44]	$C2$	192(cal) [14]	$1.17 \times KDP$	-
$CsZn_2B_3O_7$ [45,46]	$Cmc2_1$	218 [46] (<200 [45])	$1.5 \times KDP$ [46] $(3.3 \times KDP)$ [45]	0.056(cal) [46]
Borate crystals in which the B-O groups are $(BO_4)^{5-}$ groups only				
$LaBeB_3O_7$ [55]	$Pnm2_1$	220	$1\text{~}2 \times KDP$	~0.03(cal)
Borate crystals containing the B-O combinational groups				
$K_3B_6O_{10}Cl$ [57]	$R3m$	180 [57,60]	$4 \times KDP$ [57]	~0.05 (404–694 nm) [60]
$K_3B_6O_{10}Br$ [56]	$R3m$	182 [58]	$d_{22} = -1.23 \pm 0.01$ $d_{33} = 0.43 \pm 0.01$ [58] $(d_{22} = 0.83\ d_{33} = 0.51$ [59])	0.045 (0.046) [59]
$Ba_3B_6O_{11}F_2$ [63]	$P2_1$	<190	$3 \times KDP$	-
$Sr_3B_6O_{11}F_2$ [64]	$P2_1$	<190	$2.5 \times KDP$	0.04–0.047(cal) (1052–302 nm)
$GdBe_2B_5O_{11}$ [65]	$Pna2$	<200	$1 \times KDP$	-
$YBe_2B_5O_{11}$ [65]	$Pna2$	<200	$1 \times KDP$	-
The borates containing B-O groups and other NLO active groups				
$Ba_3(ZnB_5O_{10})PO_4$ [66]	$Pmn2_1$	180 [66]	$d_{powder} = 4 \times KDP$ [66]	0.033 (cal@532 nm) [66]
$Cs_2B_4SiO_9$ [67]	$I\text{-}4$	190	$4.6 \times KDP$	-
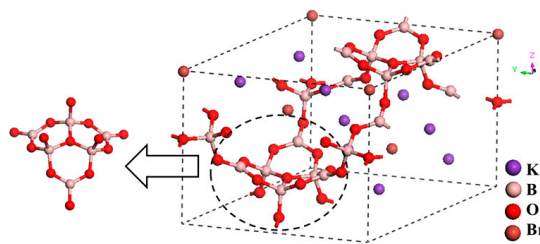
Figure 14. The structure of the $K_3B_6O_{10}Br$ and the $(B_6O_{13})^{8-}$ group.

$Ba_3B_6O_{11}F_2$ and $Sr_3B_6O_{11}F_2$ with $(B_6O_{14})^{10-}$

$Ba_3B_6O_{11}F_2$ and $Sr_3B_6O_{11}F_2$ are isomorphism and crystallize in monoclinic space group $P2_1$ [63,64]. Two $(B_3O_8)^{3-}$ are linked by sharing the oxygen of $(BO_4)^{5-}$ to form the $(B_6O_{14})^{10-}$ building block. The $(B_6O_{14})^{10-}$ groups are further interconnected to generate the 3D framework with Ba^{2+} (or Sr^{2+}) and F^+ residing in the nine-number tunnels in the framework (Figure 15). Even if some rotation occurs between the $(B_6O_{14})^{10-}$ groups, $(BO_3)^{3-}$, the basic unit mostly contributing to SHG effect, is almost in the same spatial orientation. Therefore, both crystals exhibit large SHG response (3 and 2.5 times that of KDP for $Ba_3B_6O_{11}F_2$ and $Sr_3B_6O_{11}F_2$, respectively). Besides, the formation of B-O bond between the oxygen atoms at $(BO_3)^{3-}$ group and four-coordinated boron atoms result in the absorption edge below 190 nm.
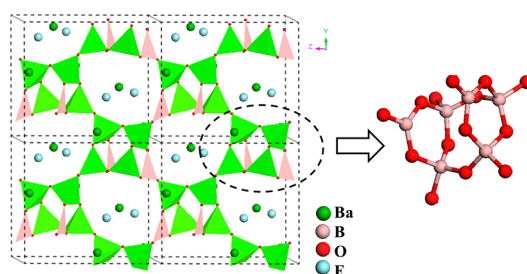
Figure 15. The structure of $Ba_3B_6O_{11}F_2$ and the $(B_6O_{14})^{10-}$ group. The $(BO_4)^{5-}$ group is represented by green tetrahedra and the $(BO_3)^{3-}$ group is represented by the pink triangle.

$ReBe_2B_5O_{11}$ (Re = Y, Gd) with $(B_4O_8)^{4-}$ chains

$YBe_2B_5O_{11}$ and $GdBe_2B_5O_{11}$ are isostructural and crystallize in space group $Pna2$ [65]. $(B_3O_7)^{5-}$ groups are interconnected by $(BO_3)^{3-}$ to generate the infinite one-dimensional $(B_4O_8)^{4-}$ chains. By sharing the corner oxygen atoms of $(BeO_4)^{6-}$ tetrahedra, $(B_4O_8)^{4-}$ chains cling to the distorted $(Be_2BO_5)_\infty$ layer, forming the $[Be_2B_5O_{11}]_\infty$ layer. The $(Be_2B_5O_{11})_\infty$ layers are aligned in a staggered manner, with the $(B_4O_8)^{4-}$ chains penetrating each other (Figure 16). The rare earth cations (Y^{3+} or Gd^{3+}) reside in the interspace between the layers (Figure 16). Due to the absence of *d-d* or *f-f* electronic transition in Y^{3+} and Gd^{3+} cations, the absorption edges of $ReBe_2B_5O_{11}$ are all below 200 nm. Powder SHG measurement showed that their SHG efficiencies are comparable with KDP. The theoretical analysis-based first-principles calculation elucidated that the large SHG response of $ReBe_2B_5O_{11}$ mainly originated from the relatively ordered spatial arrangement of $(BO_3)^{3-}$ group.
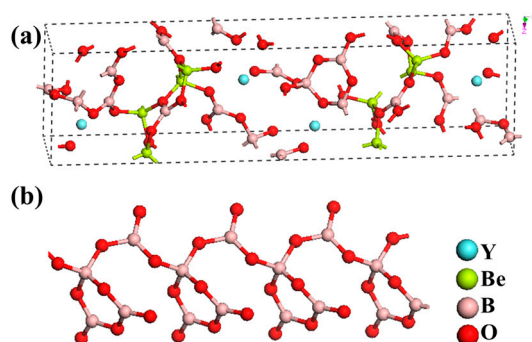
Figure 16. (**a**) The structure of $YBe_2B_5O_{11}$, (**b**) the $(B_4O_8)^{4-}$ chain projected along the c axis.

2.4. The Borates Containing B-O Groups and Other NLO Active Groups

Commonly, for the UV and DUV borate-based crystals the NLO properties mainly originate from the contribution of B-O groups. However, there exist some borates in which other types of microscopic

groups also make considerable contributions to the NLO effect apart from the B-O groups. In this section, we select $Ba_3(ZnB_5O_{10})PO_4$ and $Cs_2B_4SiO_9$ as the representative examples.

$Ba_3(ZnB_5O_{10})PO_4$

$Ba_3(ZnB_5O_{10})PO_4$ crystallizes in orthorhombic space group $Pmn2_1$ [66]. The basic building unit $(ZnB_5O_{13})^{3-}$ can be treated as the $(B_6O_{13})^{8-}$ in $K_3B_6O_{10}Cl$, with one of the four coordinated boron substituted by zinc atoms. By sharing the corner oxygen atoms, the $(ZnB_5O_{13})^{3-}$ groups are interconnected with each other to form the 3D framework (Figure 17). Barium cations and $(PO_4)^{3-}$ anions are embedded in the cavity of the framework. The measured absorption edge of is 180 nm. The introduction of $(ZnO_4)^{6-}$ into the 3D framework and $(PO_4)^{3-}$ into the cavity largely enhances the optical nonlinearity, leading to an SHG effect about $4 \times$ KDP.
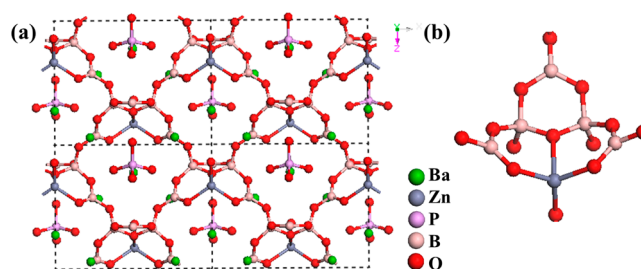
Figure 17. (a) The structure of $Ba_3(ZnB_5O_{10})PO_4$, **(b)** The basic building unit $(ZnB_5O_{13})^{3-}$ group.

$Cs_2B_4SiO_9$

$Cs_2B_4SiO_9$ crystallizes tetragonal space group *I*-4 [67]. Four $(BO_4)^{5-}$ groups are connected with each other to surround an enclosed cage-like $(B_4O_{10})^{8-}$ group. $(B_4O_{10})^{8-}$ groups are further connected by $(SiO_4)^{4-}$, forming the open three-dimensional framework. The large cesium ions are located in the cavity of the framework (Figure 18). UV/Vis–IR diffuse reflectance spectrum revealed that the absorption edge of $Cs_2B_4SiO_9$ is below 200 nm. More importantly, $Cs_2B_4SiO_9$ exhibits the largest SHG response ($4.6 \times$ KDP) in the borosilicate system, which is speculated to originate from the large distortion of the four-coordinated anion groups.
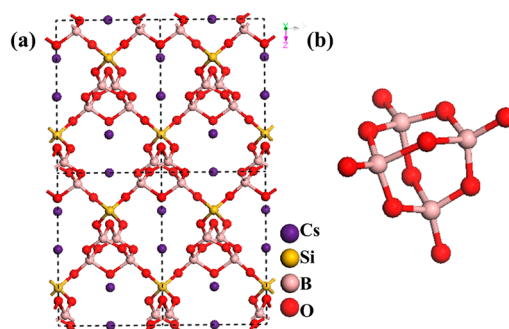
Figure 18. (a) The structure of $Cs_2B_4SiO_9$, **(b)** the $(B_4O_{10})^{8-}$ group.

3. Conclusions

In summary, the representative borate-based UV and DUV NLO crystals discovered in the recent decade are reviewed, and their structure–property relationship is analyzed. Clearly, the optical properties of these crystals are mainly determined by the spatial arrangements of $(BO_3)^{3-}$ triangles, $(BO_4)^{5-}$ tetrahedra and their combinations. In some compounds, the contribution from other types of microscopic groups, such as $(ZnO_4)^{6-}$, $(PO_4)^{3-}$ and $(SiO_4)^{4-}$, is also considerably large. The deduced mechanism understanding would have significant implications to the exploration and design of

new borate-based crystals with excellent UV NLO performance. Last, but not least, it should be emphasized that the NLO properties presented in this review are mainly based on powder samples, and re-determination by large-sized crystals is necessary in order to more accurately measure their optical performances, including birefringence values and SHG coefficients. Therefore, the crystal growth for large size crystals with high optical quality is vital for eventually evaluating the practical application prospect of NLO materials. This should also be an important research task for the practical applications of UV and DUV NLO borate in the future.

Author Contributions: Yi Yang and Xingxing Jiang wrote the paper, Zheshuai Lin designed the architecture and supervised the process of the paper, and Yicheng Wu provided scientific guidance.

Conflicts of Interest: The authors declare no conflict of interest.

References

1. Franken, P.A.; Weinreich, G.; Peters, C.W.; Hill, A.E. Generation of optical harmonics. *Phys. Rev. Lett.* **1961**, *7*, 118. [CrossRef]
2. Xu, Y.M.; Huang, Y.B.; Cui, X.Y.; Razzoli, E.; Radovic, M.; Shi, M.; Chen, G.F.; Zheng, P.; Wang, N.L.; Zhang, C.L.; et al. Observation of a ubiquitous three-dimensional superconducting gap function in optimally doped $Ba_{0.6}K_{0.4}Fe_2As_2$. *Nat. Phys.* **2011**, *7*, 198–202. [CrossRef]
3. Neil, S. Ultraviolet lasers. *Nat. Photon.* **2007**, *1*, 83–85.
4. Burland, D.M.; Miller, R.D.; Walsh, C.A. Second-Order Nonlinearity in Poled-Polymer Systems. *Chem. Rev.* **1994**, *94*, 31–75. [CrossRef]
5. Chiaverini, J.; Leibfried, D.; Schaetz, T.; Barrett, M.D.; Blakestad, R.B.; Britton, J.; Itano, W.M.; Jost, J.D.; Knill, E.; Langer, C.; et al. Nonlinear optics in the extreme ultraviolet. *Nature* **2004**, *432*, 605–608.
6. Kiss, T.; Kanetaka, F.; Yokoya, T.; Shimojima, T.; Kanai, K.; Shin, S.; Onuki, Y.; Togashi, T.; Zhang, C.; Chen, C.T.; et al. Photoemission spectroscopic evidence of gap anisotropy in an f-electron superconductor. *Phys. Rev. Lett.* **2005**, *94*, 057001. [CrossRef] [PubMed]
7. Yatsenko, L.P.; Shore, B.W.; Halfmann, T.; Bergmann, K. Source of metastable H(2s) atoms using the Stark chirped rapid-adiabatic-passage technique. *Phys. Rev. A* **1999**, *94*, R4237. [CrossRef]
8. Kiss, T.; Shimojima, T.; Kanaia, T.; Yokoya, T.; Shin, S.; Onuki, Y.; Togashi, T.; Zhang, C.; Chen, C.T. Ultrahigh-resolution photoemission spectroscopy of superconductors using a VUV laser. *J. Electron Spectrosc.* **2005**, *144*, 953–956. [CrossRef]
9. Meng, J.; Liu, G.; Zhang, W.; Zhao, L.; Liu, H.; Jia, X.; Mu, D.; Liu, S.; Dong, X.; Zhang, J.; et al. Coexistence of Fermi arcs and Fermi pockets in a high-T(c) copper oxide superconductor. *Nature* **2009**, *462*, 335–338. [CrossRef] [PubMed]
10. Balakrishnan, G.; Hu, Y.; Nielsen, S.B.; Spiro, T.G. Tunable kHz Deep Ultraviolet(193–210 nm) laser for raman applications. *Appl. Spectrosc.* **2005**, *59*, 776–781. [CrossRef] [PubMed]
11. Becker, P. Borate Materials in Nonlinear Optics. *Adv. Mater.* **1998**, *10*, 979–992. [CrossRef]
12. Chen, C.T.; Ye, N.; Lin, J.; Jiang, J.; Zeng, W.R.; Wu, B.C. Computer-assisted search for nonlinear optical crystals. *Adv. Mater.* **1999**, *11*, 1071–1078. [CrossRef]
13. Kurimura, S.; Harada, M.; Muramatsu, K.-i.; Ueda, M.; Adachi, M.; Yamada, T.; Ueno, T. Quartz revisits nonlinear optics: Twinned crystal for quasi-phase matching[Invited]. *Opt. Mater. Express* **2011**, *1*, 1367–1375. [CrossRef]
14. Jiang, X.; Luo, S.; Kang, L.; Gong, P.; Huang, H.; Wang, S.; Lin, Z.; Chen, C. First-Principles Evaluation of the Alkali and/or Alkaline Earth Beryllium Borates in Deep Ultraviolet Nonlinear Optical Applications. *ACS Photonics* **2015**, *2*, 1183–1191. [CrossRef]
15. Chen, C.T.; Sasaki, T.; Li, R.; Wu, Y.; Lin, Z.; Mori, Y.; Hu, Z.; Wang, J.; Aka, G.; Yoshimura, M.; et al. *Nonlinear Optical Borate Crystals Principals and Applications*; Wiley-VCH: New York, NY, USA, 2012.
16. Chen, C.T.; Wu, B.C.; Jiang, A.D.; You, G.M. A new-type ultraviolet SHG crystal β-BaB_2O_4. *Sci. Sin.* **1985**, *28*, 235–243.

17. Eimerl, D.; Davis, L.; Velsko, S.; Graham, E.K.; Zalkin, A. Optical, mechanical and thermal-properties of barium borate. *J. Appl. Phys.* **1987**, *62*, 1968–1983. [CrossRef]

18. Chen, C.T.; Wu, Y.C.; Jiang, A.D.; Wu, B.C.; You, G.M.; Li, R.K.; Lin, S.J. New nonlinear-optical crystal-LiB$_3$O$_5$. *J. Opt. Soc. Am. B Opt. Phys.* **1989**, *6*, 616–621. [CrossRef]

19. Chen, C.; Xu, Z.; Deng, D.; Zhang, J.; Wong, G.K. L.; Wu, B.; Ye, N.; Tang, D. The vacuum ultraviolet phase-matching characteristics of nonlinear optical KBe$_2$BO$_3$F$_2$ crystal. *Appl. Phys. Lett.* **1996**, *68*, 2930. [CrossRef]

20. Mei, L.; Huang, X.; Wang, Y.; Wu, Q.; Wu, B.; Chen, C. Crystal-structure of KBe$_2$BO$_3$F$_2$. *ZKri* **1995**, *210*, 93–95. [CrossRef]

21. Wu, B.C.; Tang, D.Y.; Ye, N.; Chen, C.T. Linear and nonlinear optical properties of the KBe$_2$BO$_3$F$_2$ (KBBF) crystal. *Opt. Mater.* **1996**, *5*, 105–109. [CrossRef]

22. Chen, C. Recent advances in deep and vacuum-UV harmonic generation with KBBF crystal. *Opt. Mater.* **2004**, *26*, 425–429. [CrossRef]

23. Chen, C.T.; Luo, S.; Wang, X.; Wang, G.L.; Wen, X.; Wu, H.; Zhang, X.; Xu, Z.Y. Deep UV nonlinear optical crystal: RbBe$_2$BO$_3$F$_2$. *J. Opt. Soc. Am. B* **2009**, *26*, 1519–1525. [CrossRef]

24. Huang, H.; Chen, C.; Wang, X.; Zhu, Y.; Wang, G.; Zhang, X.; Wang, L.; Yao, J. Ultraviolet nonlinear optical crystal: CsBe$_2$BO$_3$F$_2$. *J. Opt. Soc. Am. B* **2011**, *28*, 2186–2190. [CrossRef]

25. Kang, L.; Luo, S.; Huang, H.; Zheng, T.; Lin, Z.S.; Chen, C.T. Ab initio studies on the optical effects in the deep ultraviolet nonlinear optical crystals of the KBe$_2$BO$_3$F$_2$ family. *J. Phys. Condens. Matter.* **2012**, *24*, 335503. [CrossRef] [PubMed]

26. Chen, C.T.; Wang, G.L.; Wang, X.Y.; Xu, Z.Y. Deep-UV nonlinear optical crystal KBe$_2$BO$_3$F$_2$-discovery, growth, optical properties and applications. *Appl. Phys. B* **2009**, *97*, 9–25. [CrossRef]

27. Togashi, T.; Kanai, T.; Sekikawa, T.; Watanabe, S.; Chen, C.T.; Zhang, C.; Xu, Z.; Wang, J. Generation of vacuum-ultraviolet light by an optically contacted, prism-coupled KBe$_2$BO$_3$F$_2$ crystal. *Opt. Lett.* **2003**, *28*, 254–256. [CrossRef] [PubMed]

28. Wang, G.; Wang, X.; Zhou, Y.; Chen, Y.; Li, C.; Zhu, Y.; Xu, Z.; Chen, C. 12.95 mW sixth harmonic generation with KBe$_2$BO$_3$F$_2$ crystal. *Appl. Phys. B* **2008**, *91*, 95–97. [CrossRef]

29. Chen, C.T.; Lu, J.H.; Togashi, T.; Suganuma, T.; Sekikawa, T.; Watanabe, S.; Xu, Z.; Wang, J. Second-harmonic generation from a KBe$_2$BO$_3$F$_2$ crystal in the deep ultraviolet. *Opt. Lett.* **2002**, *27*, 637–639. [CrossRef] [PubMed]

30. Guo, S.; Jiang, X.; Liu, L.; Xia, M.; Fang, Z.; Wang, X.; Lin, Z.; Chen, C. BaBe$_2$BO$_3$F$_3$: A KBBF-Type Deep-Ultraviolet Nonlinear Optical Material with Reinforced [Be$_2$BO$_3$F$_2$]$_\infty$ Layers and Short Phase-Matching Wavelength. *Chem. Mater.* **2016**, *28*, 8871–8875. [CrossRef]

31. Huang, Q.; Liu, L.; Wang, X.; Li, R.; Chen, C. Beryllium-Free KBBF Family of Nonlinear-Optical Crystals: AZn$_2$BO$_3$X$_2$ (A = Na, K, Rb; X = Cl, Br). *Inorg. Chem.* **2016**, *55*, 12496–12499. [CrossRef] [PubMed]

32. Yang, G.; Gong, P.; Lin, Z.; Ye, N. AZn$_2$BO$_3$X$_2$(A = K, Rb, NH$_4$; X = Cl, Br): New Members of KBBF Family Exhibiting Large SHG Response and the Enhancement of Layer Interaction by Modified Structures. *Chem. Mater.* **2016**, *28*, 9122–9131. [CrossRef]

33. Chen, C.T.; Wang, Y.B.; Wu, B.C.; Wu, K.C.; Zeng, W.L.; Yu, L.H. Design and synthesis of an ultraviolet-transparent nonlinear-optical crystal Sr$_2$Be$_2$B$_2$O$_7$. *Nature* **1995**, *373*, 322–324. [CrossRef]

34. Chen, C.T.; Wang, Y.B.; Xia, Y.N.; Wu, B.C.; Tang, D.Y.; Wu, K.C.; Zeng, W.R.; Yu, L.H.; Mei, L.F. New development of nonlinear optical crystals for the ultraviolet region with molecular engineering approach. *J. Appl. Phys.* **1995**, *77*, 2268–2272. [CrossRef]

35. Meng, X.Y.; Wen, X.H.; Liu, G.L. Structure and Stacking Faults in Sr$_2$Be$_2$B$_2$O$_7$ Crystal. *J. Korean Phys. Soc.* **2008**, *52*, 1277. [CrossRef]

36. Chen, C.; Lin, Z.; Wang, Z. The development of new borate-based UV nonlinear optical crystals. *Appl. Phys. B* **2005**, *80*, 1–25. [CrossRef]

37. Huang, H.; Yao, J.; Lin, Z.; Wang, X.; He, R.; Yao, W.; Zhai, N.; Chen, C. Molecular Engineering Design to Resolve the Layering Habit and Polymorphism Problems in Deep UV NLO Crystals: New Structures in MM'Be$_2$B$_2$O$_6$F (M = Na, M' = Ca; M=K, M' = Ca, Sr). *Chem. Mater.* **2011**, *23*, 5457–5463. [CrossRef]

38. Zhao, S.; Kang, L.; Shen, Y.; Wang, X.; Asghar, M.A.; Lin, Z.; Xu, Y.; Zeng, S.; Hong, M.; Luo, J. Designing a Beryllium-Free Deep-Ultraviolet Nonlinear Optical Material without a Structural Instability Problem. *J. Am. Chem. Soc.* **2016**, *138*, 2961–2964. [CrossRef] [PubMed]

39. Zhao, S.; Gong, P.; Luo, S.; Liu, S.; Li, L.; Asghar, M.A.; Khan, T.; Hong, M.; Lin, Z.; Luo, J. Beryllium-Free $Rb_3Al_3B_3O_{10}F$ with Reinforced Inter layer Bonding as a Deep-Ultraviolet Nonlinear Optical Crystal. *J. Am. Chem. Soc.* **2015**, *137*, 2207–2210. [CrossRef] [PubMed]

40. Zhao, S.; Gong, P.; Bai, L.; Xu, X.; Zhang, S.; Sun, Z.; Lin, Z.; Hong, M.; Chen, C.; Luo, J. Beryllium-free $Li_4Sr(BO_3)_2$ for deep-ultraviolet nonlinear optical applications. *Nat. Commun.* **2014**, *5*, 4019. [CrossRef] [PubMed]

41. Huang, H.; Yao, J.; Lin, Z.; Wang, X.; He, R.; Yao, W.; Zhai, N.; Chen, C. $NaSr_3Be_3B_3O_9F_4$: A promising deep-ultraviolet nonlinear optical material resulting from the cooperative alignment of the $[Be_3B_3O_{12}F]^{10-}$ anionic group. *Angew. Chem. Int. Ed.* **2011**, *50*, 9141–9044. [CrossRef] [PubMed]

42. Wang, S.C.; Ye, N.; Li, W.; Zhao, D. Alkaline Beryllium Borate $NaBeB_3O_6$ and $ABe_2B_3O_7$ (A = K, Rb) as UV Nonlinear Optical Crystals. *J. Am. Chem. Soc.* **2010**, *132*, 8779–8786. [CrossRef] [PubMed]

43. Huang, H.W.; Liu, L.J.; Jin, S.F.; Yao, W.J.; Zhang, Y.H.; Chen, C.T. Deep-Ultraviolet Nonlinear Optical Materials: $Na_2Be_4B_4O_{11}$ and $LiNa_5Be_{12}B_{12}O_{33}$. *J. Am. Chem. Soc.* **2013**, *135*, 18319–18322. [CrossRef] [PubMed]

44. Wang, S.; Ye, N. $Na_2CsBe_6B_5O_{15}$: An Alkaline Beryllium Borate as a Deep-UV Nonlinear Optical Crystal. *J. Am. Chem. Soc.* **2011**, *133*, 11458–11461. [CrossRef] [PubMed]

45. Yu, H.; Wu, H.; Pan, S.; Yang, Z.; Hou, X.; Su, X.; Jing, Q.; Poeppelmeier, K.R.; Rondinelli, J.M. $Cs_3Zn_6B_9O_{21}$: A chemically benign member of the KBBF family exhibiting the largest second harmonic generation response. *J. Am. Chem. Soc.* **2014**, *136*, 1264–1267. [CrossRef] [PubMed]

46. Zhao, S.; Zhang, J.; Zhang, S.Q.; Sun, Z.; Lin, Z.; Wu, Y.; Hong, M.; Luo, J. A new UV nonlinear optical material $CsZn_2B_3O_7$: ZnO_4 tetrahedra double the efficiency of second-harmonic generation. *Inorg. Chem.* **2014**, *53*, 2521–2527. [CrossRef] [PubMed]

47. Tien, T.Y.; Hummel, F.A. Studies in Lithium Oxide Systems: XI, Li_2O-B_2O_3-P_2O_5. *J. Am. Ceram. Soc.* **1961**, *44*, 390–394. [CrossRef]

48. Schmidt, M.; Ewald, B.; Prots, Y.; Cardoso-Gil, R.; Armbrüster, M.; Loa, I.; Zhang, L.; Huang, Y.-X.; Schwarz, U.; Kniep, R. Growth and Characterization of BPO_4 Single Crystals. *Z. Anorg. Allg. Chem.* **2004**, *630*, 655–662. [CrossRef]

49. Li, Z.H.; Lin, Z.H.; Wu, Y.C.; Fu, P.Z.; Wang, Z.Z.; Chen, C.T. Crystal growth, optical properties measurement, and theoretical calculation of BPO_4. *Chem. Mater.* **2004**, *16*, 2906–2908. [CrossRef]

50. Zhang, X.; Wang, L.R.; Zhang, S.F.; Wang, G.L.; Zhao, S.E.; Zhu, Y.; Wu, Y.C.; Chen, C.T. Optical properties of the vacuum-ultraviolet nonlinear optical crystal-BPO_4. *J. Opt. Soc. Am. B Opt. Phys.* **2011**, *28*, 2236–2239. [CrossRef]

51. Oseledchik, Y.S.; Prosvirnin, A.L.; Starshenko, V.V.; Osadchuk, V.V.; Pisarevsky, A.I.; Belokrys, S.P.; Korol, A.S.; Svitanko, N.V.; Selevich, A.F.; Krikunov, S.A. Crystal growth and properties of strontium tetraborate. *J. Cryst. Growth* **1994**, *135*, 372–376. [CrossRef]

52. Oseledchik, Y.S.; Prosvirnin, A.L.; Pisarevskiy, A.I.; Starshenko, V.V.; Osadchuk, V.V.; Belokrys, S.P.; Svitanko, N.V.; Korol, A.S.; Krikunov, S.A.; Selevich, A.F. New nonlinear optical crystals: Strontium and lead tetraborates. *Opt. Mater.* **1995**, *4*, 669–674. [CrossRef]

53. Petrov, V.; Noack, F.; Shen, D.Z.; Pan, F.; Shen, G.Q.; Wang, X.Q.; Komatsu, R.; Alex, V. Application of the nonlinear crystal SrB_4O_7 for ultrafast diagnostics converting to wavelengths as short as 125 nm. *Opt. Lett.* **2004**, *29*, 373–375. [CrossRef] [PubMed]

54. Zaitsev, A.I.; Aleksandrovskii, A.S.; Zamkov, A.V.; Sysoev, A.M. Nonlinear optical, piezoelectric, and acoustic properties of SrB_4O_7. *Inorg. Mater.* **2006**, *42*, 1360–1362. [CrossRef]

55. Yan, X.; Luo, S.; Lin, Z.; Yue, Y.; Wang, X.; Liu, L.; Chen, C. $LaBeB_3O_7$: A new phase-matchable nonlinear optical crystal exclusively containing the tetrahedral XO_4 (X = B and Be) anionic groups. *J. Mater. Chem. C* **2013**, *1*, 3616. [CrossRef]

56. Al-Ama, A.G.; Belokoneva, E.L.; Stefanovich, S.Y.; Dimitrova, O.V.; Mochenova, N.N. Potassium bromo-borate $K_3B_6O_{10}Br$-A new nonlinear optical material. *Cryst. Rep.* **2006**, *51*, 225–230. [CrossRef]

57. Wu, H.; Pan, S.; Poeppelmeier, K.R.; Li, H.; Jia, D.; Chen, Z.; Fan, X.; Yang, Y.; Rondinelli, J.M.; Luo, H. $K_3B_6O_{10}Cl$: A new structure analogous to perovskite with a large second harmonic generation response and deep UV absorption edge. *J. Am. Chem. Soc.* **2011**, *133*, 7786–7790. [CrossRef] [PubMed]

58. Xia, M.J.; Xu, B.; Li, R.K. Growth and nonlinear optical properties of $K_3B_6O_{10}Br$ crystal. *J. Cryst. Growth* **2014**, *404*, 65–68. [CrossRef]

59. Zhang, M.; Su, X.; Pan, S.L.; Wang, Z.; Zhang, H.; Yang, Z.H.; Zhang, B.B.; Dong, L.Y.; Wang, Y.; Zhang, F.F.; Yang, Y. Linear and Nonlinear Optical Properties of $K_3B_6O_{10}Br$ Single Crystal: Experiment and Calculation. *J. Phys. Chem. C* **2014**, *118*, 11849–11856. [CrossRef]

60. Wu, H.P.; Pan, S.L.; Yu, H.W.; Jia, D.Z.; Chang, A.M.; Li, H.Y.; Zhang, F.F.; Huang, X. Growth, thermal and optical properties of a novel nonlinear optical material $K_3B_6O_{10}Cl$. *CrystEngComm* **2012**, *14*, 799–803. [CrossRef]

61. Xu, B.; Xia, M.J.; Wang, X.Y.; Li, R.K.; Chen, C.T. Second-harmonic generation at 532 nm in $K_3B_6O_{10}Br$ crystal. *Opt. Lett.* **2015**, *40*, 1073–1076. [CrossRef] [PubMed]

62. Xu, B.; Hou, Z.Y.; Xia, M.J.; Liu, L.J.; Wang, X.Y.; Li, R.K.; Chen, C.T. High average power third harmonic generation at 355 nm with $K_3B_6O_{10}Br$ crystal. *Opt. Express* **2016**, *24*, 10345–10351. [CrossRef] [PubMed]

63. Yu, H.W.; Wu, H.P.; Pan, S.L.; Yang, Z.H.; Su, X.; Zhang, F.F. A novel deep UV nonlinear optical crystal $Ba_3B_6O_{11}F_2$, with a new fundamental building block, B_6O_{14} group. *J. Mater. Chem.* **2012**, *22*, 9665–9670. [CrossRef]

64. Huang, Z.; Su, X.; Pan, S.; Dong, X.; Han, S.; Yu, H.; Zhang, M.; Yang, Y.; Cui, S.; Yang, Z. $Sr_3B_6O_{11}F_2$: A promising polar fluoroborate with short UV absorption edge and moderate second harmonic generation response. *Scr. Mater.* **2013**, *69*, 449–452. [CrossRef]

65. Yan, X.; Luo, S.; Lin, Z.; Yao, J.; He, R.; Yue, Y.; Chen, C. $ReBe_2B_5O_{11}$ (Re = Y, Gd): Rare-earth beryllium borates as deep-ultraviolet nonlinear-optical materials. *Inorg. Chem.* **2014**, *53*, 1952–1954. [CrossRef] [PubMed]

66. Yu, H.W.; Zhang, W.G.; Young, J.; Rondinelli, J.M.; Halasyamani, P.S. Design and Synthesis of the Beryllium-Free Deep-Ultraviolet Nonlinear Optical Material $Ba_3(ZnB_5O_{10})PO_4$. *Adv. Mater.* **2015**, *27*, 7380–7385. [CrossRef] [PubMed]

67. Wu, H.P.; Yu, H.W.; Pan, S.L.; Huang, Z.J.; Yang, Z.H.; Su, X.; Poeppelmeier, K.R. Cs2B4SiO9: A deep-ultraviolet nonlinear optical crystal. *Angew. Chem. Int. Ed. Engl.* **2013**, *52*, 3406–3410. [CrossRef] [PubMed]

68. Wang, G.L.; Zhang, C.Q.; Chen, C.T.; Xu, Z.Y.; Wang, J.Y. Determination of nonlinear optical coefficients of $KBe_2BO_3F_2$ crystals. *Chin. Phys. Lett.* **2003**, *20*, 243–245.